ACS OMEGA

Open Access



http://pubs.acs.org/journal/acsodf

Article

# Surface-Enhanced Raman Scattering on Size-Classified Silver Nanoparticles Generated by Laser Ablation

*Published as part of ACS Omega virtual special issue "Celebrating 50 Years of Surface Enhanced Spectroscopy".*

Soma Kenmotsu, Makoto Hirasawa, Tomoya Tamadate, Chigusa Matsumoto, Saho Osone, Yayoi Inomata, and Takafumi Seto*

Cite This: *ACS Omega* 2024, 9, 37716−37723

Read Online

ACCESS | Metrics & More | Article Recommendations

**ABSTRACT:** This study delved into the complex interplay between the nanostructural characteristics of nanoparticles and their efficacy in surface-enhanced Raman scattering (SERS) for sensitive detection of trace chemical substances. Silver nanoparticles were prepared for the SERS substrate by combining laser ablation, postannealing processes (up to 500 °C), and electrostatic mobility classification, allowing high-purity silver nanoparticles with controlling their sizes (40−100 nm) and aggregate structures. These nanoparticles were then inertially deposited on the substrates to create SERS-active surfaces, employing Rhodamine B as a probe to assess the impact of particle size, shape, and deposition density on SERS effectiveness. Our findings revealed that spherical nanoparticles, especially those approximately 50 nm in diameter, controlled to a spherical structure through gas-phase annealing at 500 °C and subsequent classification, yielded the most significant SERS enhancement. This optimal can be explained by the particle size response of the surface plasmon resonance, where the enhancement of the Raman signal for particles up to 50 nm (1/10 of the laser wavelength used in this study, 532 nm) arises from a balance between the enhancement of dipole moment and the number of "hot spot" regions (respectively proportional to the cube and inverse square of the diameters in theory, leading to a linear relationship between signal intensity and particle diameter); meanwhile, in larger size region than 50 nm, the Raman signal was decreased owing to the attribution of the phase difference between the electric field and dipole moment. Furthermore, we found that a deposition density of 2 $\mu$g resulted in nearly a single layer of particles, which is crucial for maximizing SERS hotspots and, consequently, the enhancement effect.

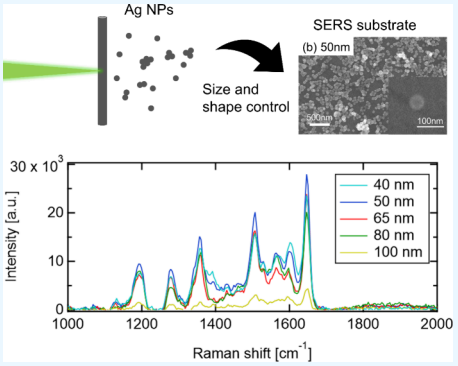


## 1. INTRODUCTION

Trace chemical substances emitted as a result of human activities have been affecting the environment and our health. Among them, organic compounds such as polycyclic aromatic hydrocarbons have a great impact on living organisms, even in very small amounts, making it necessary to establish ultrasensitive detection methods. Ultrasensitive chemical analysis at the single-molecule level, that is, single-molecule detection, has attracted attention as an analytical method for such extremely low amounts of substances in the environment. One of the methods to realize this single-molecule detection is surface-enhanced Raman scattering (SERS[1,2,6,51−55]), in which the Raman scattering signal from molecules adsorbed on noble metal nanoparticles with diameters of several tens of nanometers is significantly enhanced by surface plasmon phenomena. SERS is capable of analyzing ultralow amount components; therefore, since its principle was discovered, it has been used not only for environmental trace substances[3] but also for medical[4] and biosensing[5,6] and in a wide range of other fields. However, basic research on the elucidation of this phenomenon is required for its practical applications.[7]

One of the most important parameters determining the effectiveness of SERS is the size of metal particles. Cao et al.[8] synthesized silver nanoparticles with diameters ranging from 7 to 200 nm by wet reduction of silver nitrate and found that particles as small as 100 nm exhibit a maximum enhancement factor of $3.6 \times 10^5$. However, the resulting particles were coated with stabilizers in the liquid, and their impact on SERS was not clarified. He et al.[9] also synthesized 35−65 nm silver nanoparticles by liquid phase reduction of silver nitrate and evaluated their SERS enhancement factors. The study indicated that the impact on the performance is not only determined by the size of the silver nanoparticles but also influenced by the extent of their surface coverage on the

Received: March 29, 2024
Revised: June 16, 2024
Accepted: June 19, 2024
Published: August 25, 2024

substrate. However, the size distribution is relatively broad, and it is challenging to control two parameters, size and coverage, independently. The aggregation state of metal particles also has a significant impact on SERS; Camden et al. reported that the hot spots between particles in Ag sphere-rod dimers exhibit a very high enhancement factor.[10] Using discrete-dipole approximation simulations, they further showed that the spacing between nanospheres and rods is an important factor. These studies indicate that the design of the nanoparticle layer exhibiting SERS must include not only the particle size but also their higher-order structures. However, nanoparticles synthesized by the wet method used in many studies have difficulty controlling their morphology independently, and organic molecules, such as surface agents and ligands, are adsorbed to control particle growth, which has a marked effect on SERS sensitivity. Such surface-chemistry issues in SERS have also been noted in a review.[7]

An aerosol method is a nanoparticle synthesis in the gas phase with high purity and size and shape controllability. Our research group recently prepared three types of SERS substrates with different aggregate structures by the spray-drying method of silver nanocolloids with an average particle size of 30 nm and reported that the highest SERS effect was obtained with a structure with an aggregate diameter of 86 nm.[11] The accumulation of target molecules during the drying process has a remarkable effect on SERS sensitivity improvement, but at the same time, soluble impurities coexisting in the suspension may adsorb onto the metal particles and affect the SERS signal, as in the wet method. Therefore, it is important to construct SERS substrates with clean surfaces that are free from the effects of adsorbed impurity molecules and with controlled primary particle sizes and surface morphologies of the particle stacks. Only by using the well-controlled nanostructures, we can rigorously elucidate how these structural parameters affect the SERS. Liquid-free gas-phase methods are advantageous for fabricating such pure nanostructures.

From the perspective of reducing impurity, the laser ablation technique is advantageous for synthesizing metal nanoparticles without precursors, thus minimizing the possibility of contaminations. The laser ablation method has been applied to the preparation of SERS substrates in numerous studies conducted in both liquid[12−19] and gas (under atmospheric and vacuum conditions)[20−24] environment. Gas-phase synthesis, in particular, offers enhanced purity advantages due to negligible solvent adsorption on the particle surfaces. Hence, in this study, we employed the gas-phase laser ablation method to prepare high-purity silver nanoparticles[12,25−30] for the SERS substrate, including subsequent shape control achieved through postannealing. To further refine the particle sizes, we utilized electric mobility classification, an in-flight nanoparticle classification technique from aerosol science and technology,[31,32] resulting in a highly uniform particle size distribution with an ultranarrow standard deviation compared with previous studies.[20−24] This approach effectively addresses the challenge of achieving precise size control with ultranarrow standard deviation, facilitating the optimization of the quality and performance of the SERS substrates. The SERS substrates were fabricated by depositing these particles on substrates with a controlled density. Rhodamine B was used as the target molecule, and the effects of the size, shape, and deposition density on surface-enhanced Raman scattering were evaluated.

## 2. MATERIALS AND METHODS

### 2.1. Ag Nanoparticle Generation by Laser Ablation.

Figure 1 shows the experimental setup for generating SERS substrates with morphology-controlled Ag nanoparticles. Ag rod of 3.0 mm diameter (99.99% purity, Nilaco Co.) was used as the ablation target. A third harmonic (355 nm) nanosecond pulsed Nd:YAG laser (a pulse width of approximately 5 nm, 0.5 W, INDI-20, Spectra Physics) was focused by a lens and irradiated onto the Ag rod surface for evaporation. Nitrogen gas was continuously supplied as the carrier gas with a constant flow rate (1.5 $Lmin^{-1}$) at atmospheric pressure. The generated particles were a mixture of droplets released directly from the surface molten layer and agglomerates consisting of nanoparticles formed by vapor condensation.[33] These nanoparticles are then continuously transported in the aerosol phase.

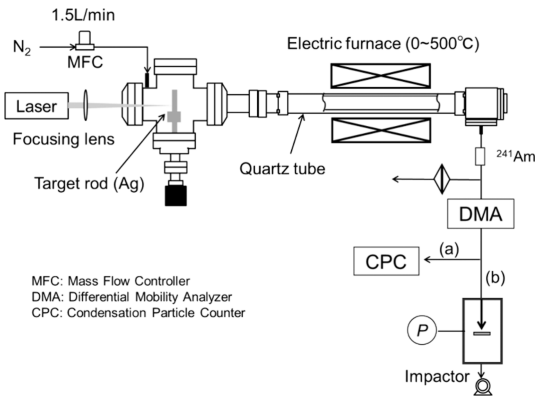


**Figure 1.** Experimental setup for preparing SERS substrates with size- and morphology-controlled Ag nanoparticles.

### 2.2. In-Flight Morphology Control and Particle Physical Properties Measurement.

Since the generated particles were a mixture of spherical particles and agglomerates of several nanometer primary particles, the morphology of the agglomerated particles was controlled by aerosol postannealing, where the channel was heated from room temperature to 500 °C using a tube-type electric furnace as shown in Figure 1. Agglomerates composed of Ag nanoparticles are known to undergo morphological changes due to sintering at temperatures significantly lower than their melting point (960 °C). We investigated the effect of this particle surface modification on SERS performance when spherization was achieved through this aerosol postannealing. When nanometer-order primary particles form an aggregate structure, the target molecules are expected to adsorb between the particles, thereby enhancing the surface effect. On the other hand, in the particle size range of approximately 1/10 of the excitation wavelength (approximately 50−100 nm) or less, the electric field enhancement effect of surface plasmons is more favorable for particles with larger particle sizes; therefore, the optimum value of SERS is considered to exist between fine primary particles with a large specific surface area and relatively large primary particles with a small specific surface area, which are expected to enhance the electric field.

To evaluate the physical properties of these annealed particles, as depicted in Figure 1a, we assessed the mobility-based particle size distributions in the aerosol state using in-flight measurements with a scanning mobility particle sizer (SMPS). The SMPS integrates an electric mobility classifier


https://doi.org/10.1021/acsomega.4c03046
ACS Omega 2024, 9, 37716−37723

(differential mobility analyzer; DMA) with a particle number concentration measuring instrument (condensation particle counter; CPC). The DMA is a well-established technique for classifying and transmitting particles with a uniform mobility diameter and narrow standard deviation.[34−37] It is noted that, for agglomerates, the DMA determines the agglomerated particle size $D_m$ as the equivalent spherical particle size based on the agglomerate's electric mobility $Z_p$, using the following equation:

$$Z_p = \frac{peC_C}{3\pi\mu D_m} \quad (1)$$

where $p$ is the number of charges, $e$ is the elementary charge, $C_C$ is Cunningham's slip correction factor, and $\mu$ is the viscosity of the gas. It is also noted that the number of charges $p$ is almost unity due to the conditioning of the charge state through the radioactive material charger ($^{241}$Am) located prior to the DMA.

As described in the following SERS substrate preparation section, we fabricated the SERS substrate using particles with size-selected by their electric mobility via the DMA. To further evaluate the primary size distribution ($D_i$) and shape of these classified particles, the postclassified particles with desired diameter were collected on a Cu substrate using an impactor. These particles were then analyzed by scanning electron microscopy (SEM; JSM-7610F, JEOL), as shown in Figure 1b.

**2.3. Preparation of SERS Substrates.** The mobility-classified particles were introduced into the impactor in a gas-floating state and ejected through a nozzle of 1.1 mm diameter to deposit on a Cu substrate (13 mm diameter, Okenshoji Co., Ltd.). The measure of inertia of the particles in the jet is given by the following Stokes number:

$$\mathrm{Stk} = \frac{\rho_p D_m^2 U}{18\mu L} \quad (2)$$

where $\rho_p$ is the particle density, $U$ is the impact velocity, and $L$ is the nozzle radius. The $U$, $C_C$, and viscosity are changed by suctioning the downstream side of the nozzle using a vacuum pump (flow rate; $Q$ = 17 Lmin$^{-1}$) to lower the pressure and temperature.[38] In this study, the pressure of the deposition chamber was set to 47.8 kPa, and the flow velocity and temperature at the nozzle outlet were calculated to be 117.8 ms$^{-1}$ and 54.6 K based on the theoretical calculations of Hering et al. Under these conditions, the particle size that satisfies the critical Stokes number ($\sqrt{\mathrm{Stk}}$ = 0.47) is 245 nm. Therefore, a single-stage impactor does not provide sufficient collection efficiency for the Ag particles (40−100 nm) targeted in this study. However, as described later in the experimental results, Ag deposition spots could be clearly observed on the Cu substrate by particle irradiation. This is thought to be due to the two-dimensional "growth" of particles deposited near the stagnation point by improving the probability of attachment of subsequent particles. Therefore, the number concentration of introduced particles was measured in real time by CPC, and the amount of particles loaded onto the impactor was precisely controlled by the deposition time. Assuming that the total particle number concentration introduced into the impactor is $N$ [m$^{-3}$] and the deposition time is $t$, the particle input amount $M$ [$\mu$g] is obtained using the following equation:

$$M = \frac{\pi}{6}\rho_p D_m^3 \times N \times 10^9 \times Q \times t \quad (3)$$

After the experiment, the Ag particle deposition spot diameter, $D_d$, was measured with an optical microscope, and the approximate particle deposition ratio, $\eta$, was determined from the following equation under conditions where the packing of a nearly single layer was confirmed by SEM.

$$\eta = \frac{\pi}{4}D_m^2 \times N \times Q \times \frac{t}{D_d} \quad (4)$$

**2.4. Target Molecule.** Rhodamine B (Rh−B, $C_{28}H_{31}ClN_2O_3$) was used as the probe molecule. The solution was diluted in ultrapure water to molar concentrations of $10^{-6}$, $10^{-7}$, and $10^{-8}$ M, and 100 $\mu$L of this solution was dropped onto the SERS substrate. The diameter of the dropped area was approximately 8 mm, and if the water completely evaporated and the molecules were uniformly dispersed and deposited on the surface, the molecular density on the surface would be $1.2 \times 10^{10}$−$10^{12}$ molecules m$^{-2}$. The spot of the Ag particles was sufficiently smaller than the drop area (approximately $\varphi$0.4 mm), and the laser irradiated area was even smaller (approximately $\varphi$1 $\mu$m). Consequently, the number of molecules in the spot for Raman scattering is considered to be 1000−100,000 or even lower than the calculated concentration because a coffee ring consisting of concentrated molecules is actually formed outside of the spot.

**2.5. Raman Spectroscopy.** Raman scattering spectroscopy analysis was performed using a microscopic Raman system consisting of an optical microscope (BX53, Olympus) and a Raman scattering spectrometer (iHR320, Horiba Ltd.). The wavelength of the excitation laser was 532 nm. The exposure time was 1 s, and the resolution of the spectrometer was 0.06 nm. The laser spot diameter was about 1 $\mu$m, and at least 10 spots where Ag particles were deposited were measured, and the maximum value was used. The variation of the peak intensity at the measured spots was about 10−15%.

## 3. RESULTS AND DISCUSSION

**3.1. Size Distribution of Generated Ag Particles.** Figure 2 shows scanning electron microscope images of Ag

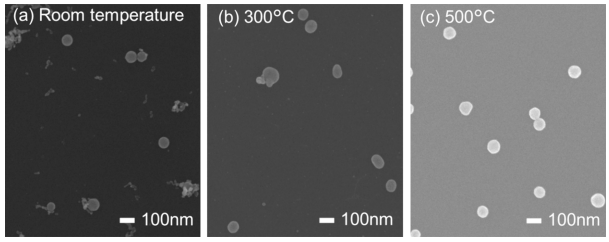


**Figure 2.** Scanning electron micrograph images of Ag (silver) particles classified in the gas phase as 80 nm in size: (a) without annealing, (b) annealed at 300 °C, and (c) annealed at 500 °C.

nanoparticles generated by laser ablation and classified as 80 nm by DMA without annealing (a), with annealing at 300 °C (b), and 500 °C (c). The particles at room temperature, which were not heated in air, are composed of many agglomerates of primary particles clearly smaller than the classified size ($D_i$ <80 nm). From the SEM image without annealing in Figure 2a, some spherical particles with nearly 80 nm in diameter are observed, likely formed by detachment from the molten layer on the target surface due to laser irradiation. Conversely,


https://doi.org/10.1021/acsomega.4c03046
ACS Omega 2024, 9, 37716−37723

agglomerates composed of primary particles several nanometers in size are also observed. These primary particles are believed to originate from the nucleation of supersaturated Ag vapor produced by laser ablation, subsequently forming the agglomerates. In the postannealed sample at 300 °C shown in Figure 2b, such agglomerates composed of small primary particles are no longer observed. Instead, some nonspherical particles are present, likely resulting from the fusion of primary particles through sintering. Increasing the annealing temperature to 500 °C further diminishes these nonspherical particles, leading to more uniform diameters due to the advanced sintering process, as depicted in Figure 2c. The particle size distribution was measured for the sample annealed at 500 °C by analyzing 200 randomly selected particles from the SEM image. The results indicated almost monodisperse particles with a mean diameter ($D_i$) of 81.6 nm and a geometric standard deviation of 1.1, which closely agrees the DMA-targeted classification diameter of 80 nm. In the classification process using the DMA, it has been noted that the charge neutralization process can produce particles with multivalent charges ($p$ >2 in eq 1), which may be mixed with univalent particles during classification.[39,40] Indeed, electron microscopy revealed the presence of some coarser particles, which contributed to an increase in the mean diameter beyond the intended classification size. However, since these particles constituted approximately 5% or less of the total particle population,[39,40] their impact on Raman scattering is considered negligible, as will be discussed later.

Figure 3 shows the particle size distribution of the aerosol, as measured by SMPS. As mentioned previously, when

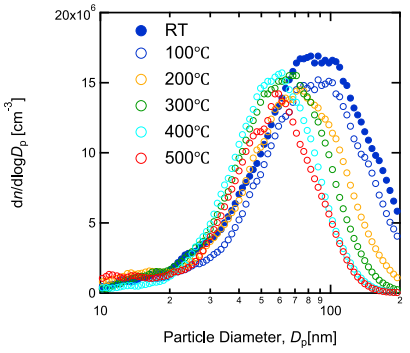


**Figure 3.** Aerosol size distribution at various postannealing temperatures ranging from room temperature (RT) up to 500 °C.

agglomerates are formed, the electric mobility diameter is larger than the primary particle diameter ($D_i < D_m$). Therefore, the particle size distribution at room temperature (no aerosol postheating) represents the mobility distribution of the agglomerates. Next, by aerosol postheating, the results indicate that the particle size distribution clearly shifts toward lower particle diameters as the heating temperature is increased. This is attributed to the densification of airborne agglomerates by sintering. In the following experiment to verify the particle size dependence in SERS, aerosols were heated in air at 500 °C, classified by DMA, and collected on a Cu substrate by an impactor.

**3.2. Surface Structure of SERS Substrate.** SEM images of monodisperse particles after air heating to 500 °C and classification are shown in Figure 4. As shown in the figure, spherical monodisperse particles were obtained for all samples.

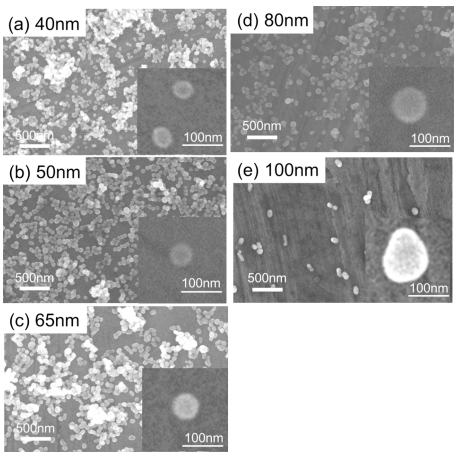


**Figure 4.** Scanning electron micrographs of monodispersed Ag particles, classified by size as (a) 40 nm, (b) 50 nm, (c) 65 nm, (d) 80 nm, and (e) 100 nm, respectively.

The mean particle sizes $D_i$ obtained from the SEM images were 44.1, 51.2, 67.5, 81.6, and 107.7 nm, respectively, and the geometric standard deviation was 1.1. Such monodisperse particles are expected to allow rigorous evaluation of the effect of particle size on SERS.

**3.3. Raman Spectroscopy Enhanced by the Size-Classified Ag Nanoparticles.** Figure 5 shows the Raman

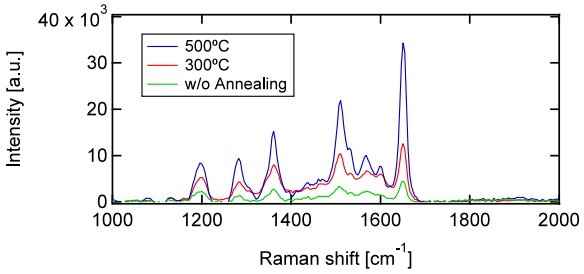


**Figure 5.** Raman spectra of the target molecules (Rh−B) of $10^{-6}$ M enhanced by 80 nm Ag particles with post annealing (at 500 and 300 °C) and without post annealing (room temperature; RT).

scattering results at different aerosol postannealing temperatures, where the Ag particle loading mass $M$ (eq 3) was maintained at 2 $\mu$g. It has been reported that the Raman scattering of Rhodamine B is obtained as a spectrum consisting of multiple peaks, starting around 1650 $cm^{-1}$, which is attributed to the C−C stretching vibration.[41,42] As shown in Figure 5, clear spectra were obtained for solutions with concentrations as low as $10^{-6}$ M, confirming the surface enhancement effect. No Raman scattering signals owing to rhodamine were obtained for the Cu substrate without Ag deposition. A comparison of the peaks around 1650 $cm^{-1}$ shows that the sample air-annealed at 500 °C resulted in the highest peak intensity, indicating that spherical particles with a larger particle size and smoother surface have a higher SERS effect. Although previous studies have demonstrated that aggregated structures often yield higher SERS intensity due to the creation of "hot spots" at the interparticle regions within the aggregates, the primary particle sizes in our study are several nanometers, which are too small to produce a pronounced SERS enhancement. This finding aligns with discussions in previous research[43−46] and is further supported


https://doi.org/10.1021/acsomega.4c03046
ACS Omega 2024, 9, 37716−37723

by the later section, size-dependent SERS response results, presented in this paper.

Figure 6 shows the effect of Ag particle size on SERS. The peak at 1650 $cm^{-1}$ was slightly higher at 50 nm than at 40 nm,

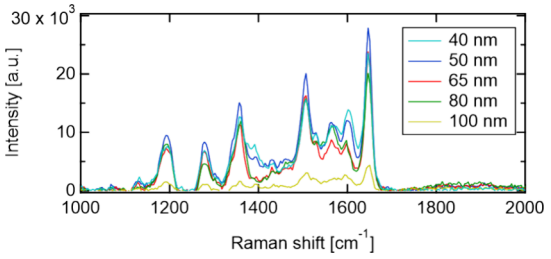


**Figure 6.** Raman spectra of Rh−B ($10^{-6}$ M) enhanced by Ag nanoparticles classified as 40, 50, 65, 80, and 100 nm, after aerosol post annealing. Raman spectra were taken by the excitation of 532 nm laser with an exposure time of 10 s.

and the peak value decreased as the particle size increased from there to 65 and 80 nm. The peak value decreased significantly when the particle size was increased to 100 nm. Therefore, we focused on the peak at 1650 $cm^{-1}$ and plotted the intensity of this peak against the particle size, yielding the results shown in Figure 7. The plot is based on the average of the five highest

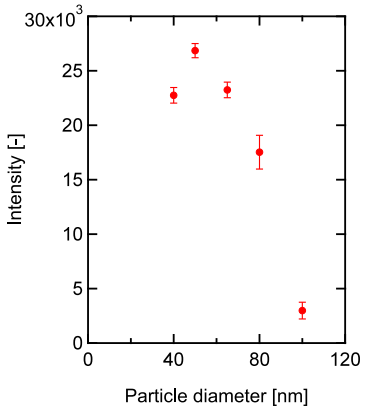


**Figure 7.** Intensity of the Raman peak at 1650 $cm^{-1}$ corresponding to the Ag particle diameter.

intensity points from the randomly measured spectra at different locations. As mentioned above, the peak intensity is the highest at 50 nm and is lower for smaller and larger sizes, which is aligned with some previous studies.[43,44]

Here, the principle of surface plasmon resonance, which is closely related to the SERS effect, is discussed. When a laser beam irradiates metal nanoparticles or metal nanostructures with a size of approximately 1/10th or less of the wavelength, the electric field of the light biases the distribution of free electrons in the nanostructure and induces an electric dipole. In such a situation, strong absorption is observed at specific wavelengths that resonate with the collective motion of free electrons; this resonance phenomenon is called surface plasmon resonance. It is known that the electric dipole moment induced on the surface of metal particles by surface plasmon resonance is proportional to the cubic of the particle size of the metal particles.[47]

Furthermore, considering the influence of the agglomerate structure of particles, there are areas called "hot spots" where significant electric field enhancement effects appear in the gaps between particles, which play an important role in high-sensitivity detection by SERS.[48] The number of hot spots in a two-dimensional layer of the size-classified particles on a substrate is inversely proportional to the projected cross-sectional area of the particles onto the substrate, i.e., the square of the particle size, under the assumption that the particles' arrangement is uniform. As a result, the SERS enhancement effect of hot spots is expected to be the product of cubic and negative squares ($D_m^3 \times D_m^{-2}$), showing a nearly linear dependence on the particle size. The SERS enhancement effect observed in Figure 7 for silver particles 40−50 nm in diameter might be attributed to this mechanism. On the other hand, the dipole moment induced in the larger particle size region (50 nm or larger) in Figure 7 is considered to be caused by the phase difference between the electric field and dipole moment. Figure 7 shows the decrease in the SERS signal observed for Ag particle sizes larger than 50 nm. Consequently, we were able to clearly demonstrate the size dependence of the SERS enhancement effect because spherical particles of uniform size were obtained by gas-phase annealing and classification. As a result, it was found that the strongest enhancement effect is obtained at 50 nm, which is almost 1/10 of the excitation wavelength of 532 nm.

To evaluate the optimum Ag structure, Figure 8 shows the results of the SEM observations of the deposition of Ag

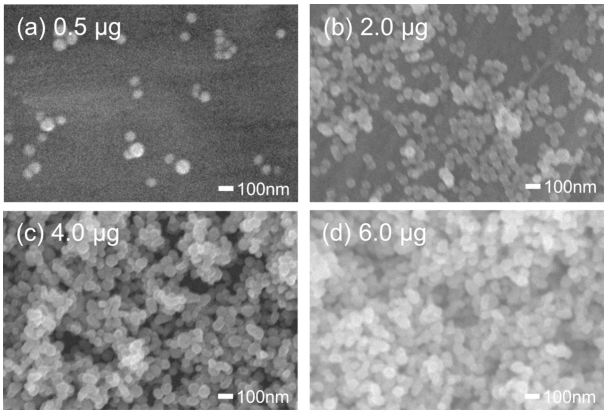


**Figure 8.** Scanning electron micrographs showing the deposition layers formed by loading (a) 0.5 $\mu$g, (b) 2.0 $\mu$g, (c) 4.0 $\mu$g, and (d) 6.0 $\mu$g of 50 nm Ag nanoparticles.

particles with a diameter of 50 nm at different introduction doses from 0.5 to 6 $\mu$g. As shown in the figure, while particles were sparsely deposited on the surface at 0.5 $\mu$g, the amount of deposited particles increased drastically at 2 $\mu$g, covering most of the area of the Cu substrate. This is thought to be due to the fact that once deposited particles improve the deposition efficiency of particles introduced later. At 2 $\mu$g, there is little overlap between the particles, and we believe that almost a single layer of particle deposition has been achieved. However, when the amount of particles introduced was further increased to 4 or 6 $\mu$g, it was confirmed that the particles overlapped each other and were further stacked in multiple layers.

Assuming that a uniform, fine-filled monolayer is formed for the deposition range diameter $D_d$ = 0.4 mm (measured value) when the input amount $M$ = 2 $\mu$g, the deposition ratios $\eta$ calculated by eq 4 are 11.7, 46.9, 95.2, and 135 for $M$ = 0.5, 2.0, 4.0, and 6.0 $\mu$g, respectively. On the other hand, the


https://doi.org/10.1021/acsomega.4c03046
ACS Omega 2024, 9, 37716−37723

surface coverage measured from the SEM images, $\eta_{exp}$, was approximately 0.11, 1.32, and 4.58, for $M$ = 0.5, 2.0, and 4.0 $\mu$g, respectively ($\eta_{exp}$ for $M$ = 6.0 was not measured because of the overlapping of particles). This difference in surface coverage might be caused by the deposition process being performed on particles smaller than the impactor cutoff diameter (245 nm). It is thought that, by depositing at a lower yield (1/100−1/20), more SERS hot spots were created due to the particle surface migration and growth at smaller spots near the stagnation point of the impactor jet. The deposition time in this study ranged from 2 to 85 min, depending on the particle size (classified value) and concentration (real-time measured value). However, using more efficient collection methods, such as low-pressure impactors and electrostatic deposition methods, the production yield of the SERS substrate may be scaled up by 50 times or more. Additionally, regarding the discussion on the number of layers, the impactor deposition method used in this study placed particles on the substrate without positional regulation, making it challenging to achieve a completely uniform layer. Therefore, the number of layers mentioned in this study is noted merely as an indicator for determining the amount of Ag nanoparticle accumulation. If a methodology enabling controlled layer deposition is developed, further improvements in the SERS effect are anticipated in the future.

Raman scattering of 50 nm Ag particles with different amounts of Ag particles introduced under the same conditions as before yields the results shown in Figure 9. The peaks

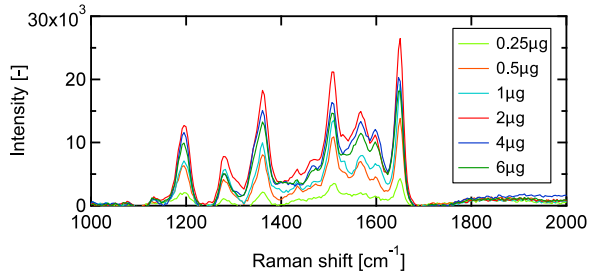


**Figure 9.** Raman spectra of Rh−B at a concentration of $10^{-6}$ M, enhanced by a SERS substrate prepared with Ag nanoparticles sized 50 nm, with varying loading amounts.

increase up to 2 $\mu$g, where almost one layer of deposition is confirmed, but when the amount of Ag particles introduced is increased to 4 $\mu$g or more, the peak height conversely decreases, as shown in Figure 9. This may be due to the fact that the dropped Rh−B penetrated into the inside of the multilayered particle layers, which reduced the efficiency of the Raman scattering analysis.

From the above-mentioned experimental results, under our experimental conditions, the optimal SERS substrate was prepared by depositing 50 nm Ag particles with a mass loading of 2 $\mu$g. Therefore, we finally attempted to detect even lower concentrations of Rh−B using our best SERS substrates fabricated under these conditions. The results are shown in Figure 10. Figure 10a shows that, even at $10^{-7}$ M, a sufficient signal of Rh−B was observed, furthermore, in Figure 10b, a peak at 1620 $cm^{-1}$ is observed even at a very low concentration of $10^{-8}$ M. In both cases, some peaks of unknown origin were observed, e.g., at 1400 and 1600 $cm^{-1}$ in Figure 10a. It potentially due to the slight contamination during the washing of the copper substrate, resulting in the detection of trace

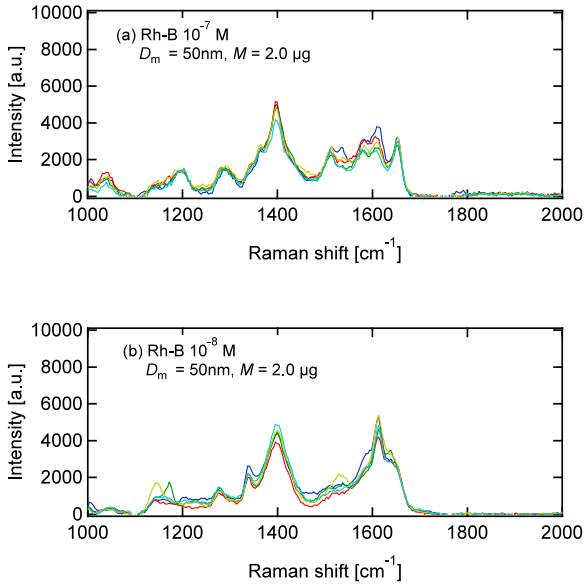


**Figure 10.** Raman spectra of Rh−B at a concentration of (a) $10^{-7}$ M, and (b) $10^{-8}$ M enhanced by a SERS substrate prepared with Ag nanoparticles sized 50 nm with a loading amount of 2.0 $\mu$g.

amounts of contaminants (such as something organic residuals), although we minimized the contamination of organic compounds as much as possible. Also, the line shapes observed in each tracer concentration are different, specifically in 1620 $cm^{-1}$ peak $10^{-8}$ M intensity is equal or higher than $10^{-7}$ M. This nonlinear phenomenon (intensity vs analyte concentration) is still unknown, but it is potentially occurred by the contacting of the analytes each other during the evaporation process at higher concentration, decreasing the effective analyte concentration. The other possibility is the orientation of the molecules on the Ag nanoparticles were different in different evaporation processes because of the variation of evaporation processes, affecting the enhancement as discussed in previous studies.[49,50] In terms of the detection limit, previous studies have reported more ultrasensitive SERS substrate preparation methods capable of detecting Rhodamine 6G concentrations ranging from $10^{-13}$ to $10^{-20}$ M with special techniques, e.g., precise control of SERS platform hydrophilic/phobic properties,[51,52] employing the silver-mirror reaction,[6] coating Ag nanolayers onto self-assembled $SiO_2$ particles,[53] synthesizing Ag nanoparticles within a mesoporous silicon matrix,[54] combining the e-beam lithography and electroless deposition.[55] Meanwhile, in this paper, we investigate methodology to optimize SERS efficiency by focusing on particle density on the SERS substrate and a wide dynamic range of particle sizes with narrow standard deviation, with applying a commonly used excitation wavelength of 532 nm for detecting Rhodamine 6G. Given the consideration of method universality, a detection limit of $10^{-8}$ M demonstrates sufficiently high sensitivity for practical applications.

## 4. SUMMARY

Impurity-free silver nanoparticles were generated using a laser ablation method and applied as SERS substrates. The experiments showed that spherical particles with smooth surfaces produced a higher SERS effect. Furthermore, the SERS effect varied greatly depending on the particle size and


https://doi.org/10.1021/acsomega.4c03046
ACS Omega 2024, 9, 37716−37723

amount of particles deposited on the substrate, and it was found that the highest enhancement effect was obtained with substrates prepared by depositing 2 μg (almost monolayer) of 50 nm Ag nanoparticles.

## AUTHOR INFORMATION


### Corresponding Author

**Takafumi Seto** − *School of Frontier Engineering, Kanazawa University, Kanazawa 920-1192, Japan*; orcid.org/0000-0002-7821-7096; Email: t.seto@staff.kanazawa-u.ac.jp

### Authors

**Soma Kenmotsu** − *School of Frontier Engineering, Kanazawa University, Kanazawa 920-1192, Japan*

**Makoto Hirasawa** − *National Institute of Advanced Science and Technology (AIST), Tsukuba 305-8560, Japan*

**Tomoya Tamadate** − *School of Frontier Engineering, Kanazawa University, Kanazawa 920-1192, Japan*

**Chigusa Matsumoto** − *School of Frontier Engineering, Kanazawa University, Kanazawa 920-1192, Japan*

**Saho Osone** − *School of Frontier Engineering, Kanazawa University, Kanazawa 920-1192, Japan*

**Yayoi Inomata** − *School of Frontier Engineering, Kanazawa University, Kanazawa 920-1192, Japan*; orcid.org/0000-0003-3570-545X

Complete contact information is available at: https://pubs.acs.org/10.1021/acsomega.4c03046


### Notes

The authors declare no competing financial interest.

## ACKNOWLEDGMENTS

This work was supported by JST CREST Grant Number JPMJCR18H4, Japan, and KAKENHI JP21H01687 and JP24K01232.

## REFERENCES


(1) Fleischmann, M.; Hendra, P. J.; McQuillan, A. J. Raman Spectra of Pyridine Adsorbed at a Silver Electrode. *Chem. Phys. Lett.* **1974**, *26* (2), 163−166.

(2) Kneipp, K.; Wang, Y.; Kneipp, H.; Perelman, L. T.; Itzkan, I.; Dasari, R. R.; Feld, M. S. Single Molecule Detection Using Surface-Enhanced Raman Scattering (SERS). *Phys. Rev. Lett.* **1997**, *78* (9), 1667−1670.

(3) Schmidt, H.; Bich Ha, N.; Pfannkuche, J.; Amann, H.; Kronfeldt, H.-D.; Kowalewska, G. Detection of PAHs in Seawater Using Surface-Enhanced Raman Scattering (SERS). *Mar. Pollut. Bull.* **2004**, *49* (3), 229−234.

(4) Cialla-May, D.; Zheng, X.-S.; Weber, K.; Popp, J. Recent Progress in Surface-Enhanced Raman Spectroscopy for Biological and Biomedical Applications: From Cells to Clinics. *Chem. Soc. Rev.* **2017**, *46* (13), 3945−3961.

(5) Pilot; Signorini; Durante; Orian; Bhamidipati; Fabris. A Review on Surface-Enhanced Raman Scattering. *Biosensors (Basel)* **2019**, *9* (2), 57.

(6) Mazur, N. V.; Kapush, O. A.; Isaeva, O. F.; Budzulyak, S. I.; Buziashvili, A. Yu.; Pirko, Y. V.; Skoryk, M. A.; Yemets, A. I.; Hreshchuk, O. M.; Yukhymchuk, V.; Dzhagan, V. M. Facile SERS Substrates from Ag Nanostructures Chemically Synthesized on Glass Surfaces. *Physics and Chemistry of Solid State* **2023**, *24* (4), 682−691.

(7) Langer, J.; Jimenez de Aberasturi, D.; Aizpurua, J.; Alvarez-Puebla, R. A.; Auguié, B.; Baumberg, J. J.; Bazan, G. C.; Bell, S. E. J.; Boisen, A.; Brolo, A. G.; Choo, J.; Cialla-May, D.; Deckert, V.; Fabris, L.; Faulds, K.; García de Abajo, F. J.; Goodacre, R.; Graham, D.; Haes, A. J.; Haynes, C. L.; Huck, C.; Itoh, T.; Käll, M.; Kneipp, J.; Kotov, N. A.; Kuang, H.; Le Ru, E. C.; Lee, H. K.; Li, J.-F.; Ling, X. Y.; Maier, S. A.; Mayerhöfer, T.; Moskovits, M.; Murakoshi, K.; Nam, J.-M.; Nie, S.; Ozaki, Y.; Pastoriza-Santos, I.; Perez-Juste, J.; Popp, J.; Pucci, A.; Reich, S.; Ren, B.; Schatz, G. C.; Shegai, T.; Schlücker, S.; Tay, L.-L.; Thomas, K. G.; Tian, Z.-Q.; Van Duyne, R. P.; Vo-Dinh, T.; Wang, Y.; Willets, K. A.; Xu, C.; Xu, H.; Xu, Y.; Yamamoto, Y. S.; Zhao, B.; Liz-Marzán, L. M. Present and Future of Surface-Enhanced Raman Scattering. *ACS Nano* **2020**, *14* (1), 28−117.

(8) Cao, Y.; Zheng, R.; Ji, X.; Liu, H.; Xie, R.; Yang, W. Syntheses and Characterization of Nearly Monodispersed, Size-Tunable Silver Nanoparticles over a Wide Size Range of 7−200 Nm by Tannic Acid Reduction. *Langmuir* **2014**, *30* (13), 3876−3882.

(9) He, R. X.; Liang, R.; Peng, P.; Zhou, Y. N. Effect of the Size of Silver Nanoparticles on SERS Signal Enhancement. *J. Nanopart. Res.* **2017**, *19* (8), 267 DOI: 10.1007/s11051-017-3953-0.

(10) Camden, J. P.; Dieringer, J. A.; Wang, Y.; Masiello, D. J.; Marks, L. D.; Schatz, G. C.; Van Duyne, R. P. Probing the Structure of Single-Molecule Surface-Enhanced Raman Scattering Hot Spots. *J. Am. Chem. Soc.* **2008**, *130* (38), 12616−12617.

(11) Matsumoto, C.; Gen, M.; Matsuki, A.; Seto, T. Development of Spray-Drying-Based Surface-Enhanced Raman Spectroscopy. *Sci. Rep.* **2022**, *12* (1), 4511 DOI: 10.1038/s41598-022-08598-y.

(12) Talaikis, M.; Mikoliunaite, L.; Gkouzi, A.-M.; Petrikaitė, V.; Stankevičius, E.; Drabavičius, A.; Selskis, A.; Juškėnas, R.; Niaura, G. Multiwavelength SERS of Magneto-Plasmonic Nanoparticles Obtained by Combined Laser Ablation and Solvothermal Methods. *ACS Omega* **2023**, *8* (51), 49396−49405.

(13) Giorgetti, E.; Muniz-Miranda, M.; Marsili, P.; Scarpellini, D.; Giammanco, F. Stable Gold Nanoparticles Obtained in Pure Acetone by Laser Ablation with Different Wavelengths. *J. Nanopart. Res.* **2012**, *14* (1), 648.

(14) Olea-Mejía, O.; Fernández-Mondragón, M.; Rodríguez-de la Concha, G.; Camacho-López, M. SERS-Active Ag, Au and Ag−Au Alloy Nanoparticles Obtained by Laser Ablation in Liquids for Sensing Methylene Blue. *Appl. Surf. Sci.* **2015**, *348*, 66−70.

(15) Zhou, L.; Zhang, H.; Bao, H.; Liu, G.; Li, Y.; Cai, W. Onion-Structured Spherical $MoS_2$ Nanoparticles Induced by Laser Ablation in Water and Liquid Droplets' Radial Solidification/Oriented Growth Mechanism. *J. Phys. Chem. C* **2017**, *121* (41), 23233−23239.

(16) Gurbatov, S.; Puzikov, V.; Modin, E.; Shevlyagin, A.; Gerasimenko, A.; Mitsai, E.; Kulinich, S. A.; Kuchmizhak, A. Ag-Decorated Si Microspheres Produced by Laser Ablation in Liquid: All-in-One Temperature-Feedback SERS-Based Platform for Nanosensing. *Materials* **2022**, *15* (22), 8091.

(17) Byram, C.; Rathod, J.; Moram, S. S. B.; Mangababu, A.; Soma, V. R. Picosecond Laser-Ablated Nanoparticles Loaded Filter Paper for SERS-Based Trace Detection of Thiram, 1,3,5-Trinitroperhydro-1,3,5-Triazine (RDX), and Nile Blue. *Nanomaterials* **2022**, *12* (13), 2150.

(18) Mangababu, A.; Sai Prasad Goud, R.; Byram, C.; Rathod, J.; Banerjee, D.; Rao Soma, V.; Nageswara Rao, S. V. S. Multi-Functional Gallium Arsenide Nanoparticles and Nanostructures Fabricated Using Picosecond Laser Ablation. *Appl. Surf. Sci.* **2022**, *589*, No. 152802.

(19) Verma, A. K.; Soni, R. K. Laser Ablation Synthesis of Bimetallic Gold-Palladium Core@shell Nanoparticles for Trace Detection of Explosives. *Opt Laser Technol.* **2023**, *163*, No. 109429.

(20) Liu, J.; Wang, Z.; Meng, Y.; Chen, C.; Chen, Q.; Wang, Y.; Dou, S.; Liu, X.; Lu, N. Increasing Hotspots Density for High-Sensitivity SERS Detection by Assembling Array of Ag Nanocubes. *Talanta* **2023**, *258*, No. 124408.

(21) Smyth, C. A.; Mirza, I.; Lunney, J. G.; McCabe, E. M. Surface-Enhanced Raman Spectroscopy (SERS) Using Ag Nanoparticle Films Produced by Pulsed Laser Deposition. *Appl. Surf. Sci.* **2013**, *264*, 31−35.

(22) Khan, T. M.; Lunney, J. G.; O'Rourke, D.; Meyer, M.-C.; Creel, J. R.; Siewierska, K. E. Various Pulsed Laser Deposition Methods for Preparation of Silver-Sensitised Glass and Paper Substrates for Surface-Enhanced Raman Spectroscopy. *Appl. Phys. A: Mater. Sci. Process.* **2019**, *125* (9), 659.

(23) Budner, B.; Kuźma, M.; Nasiłowska, B.; Bartosewicz, B.; Liszewska, M.; Jankiewicz, B. J. Fabrication of Silver Nanoisland Films by Pulsed Laser Deposition for Surface-Enhanced Raman Spectroscopy. *Beilstein Journal of Nanotechnology* **2019**, *10*, 882−893.
(24) Jing, Y.; Wang, H.; Zhao, J.; Yi, H.; Wang, X. Pulsed Laser Deposition of Ag Nanoparticles on Titanium Hydroxide/Oxide Nanobelt Arrays for Highly Sensitive Surface-Enhanced Raman Spectroscopy. *Appl. Surf. Sci.* **2015**, *347*, 499−504.
(25) Kim, M.; Osone, S.; Kim, T.; Higashi, H.; Seto, T. Synthesis of Nanoparticles by Laser Ablation: A Review. *KONA Powder and Particle Journal* **2017**, *34* (0), 80−90.
(26) Tsuji, T.; Iryo, K.; Watanabe, N.; Tsuji, M. Preparation of Silver Nanoparticles by Laser Ablation in Solution: Influence of Laser Wavelength on Particle Size. *Appl. Surf. Sci.* **2002**, *202* (1−2), 80−85.
(27) Rhim, J.-W.; Wang, L.-F.; Lee, Y.; Hong, S.-I. Preparation and Characterization of Bio-Nanocomposite Films of Agar and Silver Nanoparticles: Laser Ablation Method. *Carbohydr. Polym.* **2014**, *103*, 456−465.
(28) Mafuné, F.; Kohno, J. Y.; Takeda, Y.; Kondow, T.; Sawabe, H. Formation and Size Control of Silver Nanoparticles by Laser Ablation in Aqueous Solution. *J. Phys. Chem. B* **2000**, *104* (39), 9111−9117.
(29) Mafuné, F.; Kohno, J.; Takeda, Y.; Kondow, T.; Sawabe, H. Structure and Stability of Silver Nanoparticles in Aqueous Solution Produced by Laser Ablation. *J. Phys. Chem. B* **2000**, *104* (35), 8333−8337.
(30) Petrikaitė, V.; Skapas, M.; Stankevičius, E. Generation of Gold and Silver Nanoparticles Using Laser Ablation of Thin Bimetallic Films and Bulk Targets in Water. *Opt Mater. (Amst)* **2023**, *137*, No. 113535.
(31) Knutson, E. O.; Whitby, K. T. Aerosol Classification by Electric Mobility: Apparatus, Theory, and Applications. *J. Aerosol Sci.* **1975**, *6* (6), 443−451.
(32) Intra, P.; Tippayawong, N. An Overview of Differential Mobility Analyzers for Size Classification of Nanometer-Sized Aerosol Particles. *Songklanakarin J. Sci. Technol.* **2008**, *30* (2), 243−256.
(33) Kawakami, Y.; Seto, T.; Yoshida, T.; Ozawa, E. Gold Nanoparticles and Films Produced by a Laser Ablation/Gas Deposition (LAGD) Method. *Appl. Surf. Sci.* **2002**, *197*−*198*, 587−593.
(34) Karlsson, L. S.; Deppert, K.; Malm, J.-O. Size Determination of Au Aerosol Nanoparticles by Off-Line TEM/STEM Observations. *J. Nanopart. Res.* **2006**, *8* (6), 971−980.
(35) Hirasawa, M.; Orii, T.; Seto, T. Effect of Insitu Annealing on Physical Properties of Si Nanoparticles Synthesized by Pulsed Laser Ablation. *Appl. Phys. A: Mater. Sci. Process.* **2004**, *79* (4−6), 1421−1424.
(36) Sakiyama, K.; Koga, K.; Seto, T.; Hirasawa, M.; Orii, T. Formation of Size-Selected Ni/NiO Core−Shell Particles by Pulsed Laser Ablation. *J. Phys. Chem. B* **2004**, *108* (2), 523−529.
(37) Chen, D.-R.; Pui, D. Y. H.; Mulholland, G. W.; Fernandez, M. DESIGN AND TESTING OF AN AEROSOL/SHEATH INLET FOR HIGH RESOLUTION MEASUREMENTS WITH A DMA. *J. Aerosol Sci.* **1999**, *30* (8), 983−999.
(38) Hering, S. V. Calibration of the QCM Impactor for Stratospheric Sampling. *Aerosol Sci. Technol.* **1987**, *7* (3), 257−274.
(39) Wiedensohler, A. An Approximation of the Bipolar Charge Distribution for Particles in the Submicron Size Range. *J. Aerosol Sci.* **1988**, *19* (3), 387−389.
(40) Adachi, M.; Kousaka, Y.; Okuyama, K. Unipolar and Bipolar Diffusion Charging of Ultrafine Aerosol Particles. *J. Aerosol Sci.* **1985**, *16* (2), 109−123.
(41) Zhang, J.; Li, X.; Sun, X.; Li, Y. Surface Enhanced Raman Scattering Effects of Silver Colloids with Different Shapes. *J. Phys. Chem. B* **2005**, *109* (25), 12544−12548.
(42) Hildebrandt, P.; Stockburger, M. Surface-Enhanced Resonance Raman Spectroscopy of Rhodamine 6G Adsorbed on Colloidal Silver. *J. Phys. Chem.* **1984**, *88* (24), 5935−5944.
(43) Hong, S.; Li, X. Optimal Size of Gold Nanoparticles for Surface-Enhanced Raman Spectroscopy under Different Conditions. *J. Nanomater* **2013**, *2013*, 1−9.
(44) Stamplecoskie, K. G.; Scaiano, J. C.; Tiwari, V. S.; Anis, H. Optimal Size of Silver Nanoparticles for Surface-Enhanced Raman Spectroscopy. *J. Phys. Chem. C* **2011**, *115* (5), 1403−1409.
(45) Njoki, P. N.; Lim, I.-I. S.; Mott, D.; Park, H.-Y.; Khan, B.; Mishra, S.; Sujakumar, R.; Luo, J.; Zhong, C.-J. Size Correlation of Optical and Spectroscopic Properties for Gold Nanoparticles. *J. Phys. Chem. C* **2007**, *111* (40), 14664−14669.
(46) Pal, P.; Bonyár, A.; Veres, M.; Himics, L.; Balázs, L.; Juhász, L.; Csarnovics, I. A Generalized Exponential Relationship between the Surface-Enhanced Raman Scattering (SERS) Efficiency of Gold/Silver Nanoisland Arrangements and Their Non-Dimensional Interparticle Distance/Particle Diameter Ratio. *Sens Actuators A Phys.* **2020**, *314*, No. 112225.
(47) Wakaki, M.; Yokoyama, E. Optical Properties of Oxide Films Dispersed with Nanometal Particles. In *UV-VIS and Photoluminescence Spectroscopy for Nanomaterials Characterization*; Springer: Berlin Heidelberg: Berlin, Heidelberg, 2013; pp 311−356. DOI: 10.1007/978-3-642-27594-4_8.
(48) Futamata, M.; Maruyama, Y.; Ishikawa, M. Adsorbed Sites of Individual Molecules on Ag Nanoparticles in Single Molecule Sensitivity - Surface-Enhanced Raman Scattering. *J. Phys. Chem. B* **2004**, *108* (35), 13119−13127.
(49) Dzhagan, V.; Mazur, N.; Smirnov, O.; Yeshchenko, O.; Isaieva, O.; Kovalenko, M.; Vuichyk, M.; Skoryk, M.; Pirko, Y.; Yemets, A.; Yukhymchuk, V.; Valakh, M. SERS Application of Ag Nanoparticles Synthesized with Aqueous Fungi Extract. *J. Nanopart. Res.* **2023**, *25* (3), 37.
(50) Shiohara, A.; Wang, Y.; Liz-Marzán, L. M. Recent Approaches toward Creation of Hot Spots for SERS Detection. *Journal of Photochemistry and Photobiology C: Photochemistry Reviews* **2014**, *21*, 2−25.
(51) Luo, X.; Pan, R.; Cai, M.; Liu, W.; Chen, C.; Jiang, G.; Hu, X.; Zhang, H.; Zhong, M. Atto-Molar Raman Detection on Patterned Superhydrophilic-Superhydrophobic Platform via Localizable Evaporation Enrichment. *Sens Actuators B Chem.* **2021**, *326*, No. 128826.
(52) Yu, J.; Wu, J.; Yang, H.; Li, P.; Liu, J.; Wang, M.; Pang, J.; Li, C.; Yang, C.; Xu, K. Extremely Sensitive SERS Sensors Based on a Femtosecond Laser-Fabricated Superhydrophobic/-Philic Microporous Platform. *ACS Appl. Mater. Interfaces* **2022**, *14* (38), 43877−43885.
(53) Dzhagan, V.; Mazur, N.; Kapush, O.; Skoryk, M.; Pirko, Y.; Yemets, A.; Dzhahan, V.; Shepeliavyi, P.; Valakh, M.; Yukhymchuk, V. Self-Organized SERS Substrates with Efficient Analyte Enrichment in the Hot Spots. *ACS Omega* **2024**, *9* (4), 4819−4830.
(54) Virga, A.; Rivolo, P.; Frascella, F.; Angelini, A.; Descrovi, E.; Geobaldo, F.; Giorgis, F. Silver Nanoparticles on Porous Silicon: Approaching Single Molecule Detection in Resonant SERS Regime. *J. Phys. Chem. C* **2013**, *117* (39), 20139−20145.
(55) Coluccio, M. L.; Das, G.; Mecarini, F.; Gentile, F.; Pujia, A.; Bava, L.; Tallerico, R.; Candeloro, P.; Liberale, C.; De Angelis, F.; Di Fabrizio, E. Silver-Based Surface Enhanced Raman Scattering (SERS) Substrate Fabrication Using Nanolithography and Site Selective Electroless Deposition. *Microelectron. Eng.* **2009**, *86* (4−6), 1085−1088.


https://doi.org/10.1021/acsomega.4c03046
*ACS Omega* 2024, 9, 37716−37723